Monthly Notices of the ROYAL ASTRONOMICAL SOCIETY

MNRAS **475,** 4020–4026 (2018) doi:10.1093/mnras/sty073
Advance Access publication 2018 January 10

# Do satellite galaxies trace matter in galaxy clusters?

Chunxiang Wang,[1,2★] Ran Li,[1,3★] Liang Gao,[1,3,4] Huanyuan Shan,[5,6] Jean-Paul Kneib,[5,7] Wenting Wang,[8] Gang Chen,[2] Martin Makler,[9] Maria E. S. Pereira,[9,10] Lin Wang,[1,3] Marcio A. G. Maia[11] and Thomas Erben[6]

[1]*Key Laboratory for Computational Astrophysics, National Astronomical Observatories, Chinese Academy of Sciences, Beijing 100012, China*
[2]*Tianjin Astrophysics Center, Tianjin Normal University, Tianjin 300387, China*
[3]*School of Astronomy and Space Sciences, University of Chinese Academy of Sciences, 19A Yuquan Road, Beijing 100049, China*
[4]*Institute of Computational Cosmology, Department of Physics, University of Durham, Science Laboratories, South Road, Durham DH1 3LE, UK*
[5]*Laboratoire d'astrophysique (LASTRO), Ecole Polytechnique Fédérale de Lausanne (EPFL), Observatoire de Sauverny, CH-1290 Versoix, Switzerland*
[6]*Argelander Institute for Astronomy, University of Bonn, Auf dem Hügel 71, D-53121 Bonn, Germany*
[7]*Aix Marseille Université, CNRS, LAM (Laboratoire d'Astrophysique de Marseille) UMR 7326, F-13388, Marseille, France*
[8]*Kavli IPMU (WPI), UTIAS, The University of Tokyo, Kashiwa, Chiba 277-8583, Japan*
[9]*Centro Brasileiro de Pesquisas Físicas-Rua Dr. Xavier Sigaud 150, CEP 22290-180, Rio de Janeiro, RJ, Brazil*
[10]*Brandeis University, 415 South Street, Waltham, MA 02453, USA*
[11]*Laboratório Interinstitucional de e-Astronomia-LIneA, Rua General José Cristino, 77, Rio de Janeiro, RJ, 20921-400, Brazil*

Accepted 2018 January 5. Received 2017 December 11; in original form 2017 June 18

## ABSTRACT

The spatial distribution of satellite galaxies encodes rich information of the structure and assembly history of galaxy clusters. In this paper, we select a red-sequence Matched-filter Probabilistic Percolation cluster sample in SDSS Stripe 82 region with $0.1 \leq z \leq 0.33$, $20 < \lambda < 100$, and $P_{\rm cen} > 0.7$. Using the high-quality weak lensing data from CS82 Survey, we constrain the mass profile of this sample. Then we compare directly the mass density profile with the satellite number density profile. We find that the total mass and number density profiles have the same shape, both well fitted by an NFW profile. The scale radii agree with each other within a $1\sigma$ error ($r_{\rm s,gal} = 0.34^{+0.04}_{-0.03}$ Mpc versus $r_{\rm s} = 0.37^{+0.15}_{-0.10}$ Mpc).

**Key words:** gravitational lensing: weak – galaxies: clusters: general – galaxies: statistics – dark matter.

## 1 INTRODUCTION

The spatial distribution of satellite galaxies encodes rich information of the structure of galaxy clusters/groups. In particular, the radial number density profiles of galaxy clusters have been often used to constrain galaxy formation models (e.g. Diemand, Moore & Stadel 2004; Gao et al. 2004; Wang et al. 2014). High-resolution simulations show that the distribution of subhaloes is less concentrated than the distribution of dark matter (Springel et al. 2001; Gao et al. 2004; Vogelsberger et al. 2014). In addition, subhaloes appear to have a significantly shallower radial distribution than the observed distribution of galaxies in the inner region of clusters (Gao et al. 2004). In hydrodynamical simulations, the galaxies can survive longer than the dark matter subhaloes. The dissipative processes of galaxy formation make the stellar component more resistant to tidal disruption close to cluster centres (Vogelsberger et al. 2014). Observationally, there are lots of controversies in the literature on whether satellite galaxies unbiasedly trace the underlying mass distribution in galaxy clusters/groups. Some studies conclude that the satellite (luminosity) distribution traces the mass distribution (Tyson & Fischer 1995; Squires et al. 1996; Carlberg, Yee & Ellingson 1997; Cirimele, Nesci & Trèvese 1997; Fischer & Tyson 1997; van der Marel et al. 2000; Rines et al. 2001; Tustin et al. 2001; Biviano & Girardi 2003; Łokas & Mamon 2003; Kneib et al. 2003; Parker et al. 2005; Popesso et al. 2007; Sheldon et al. 2009; Sereno, Lubini & Jetzer 2010; Wojtak & Łokas 2010; Bahcall & Kulier 2014); while some studies suggest that the spatial distribution of satellites (luminosity) is less concentrated than that of matter (Rines et al. 2000; Lin, Mohr & Stanford 2004; Hansen et al. 2005; Nagai & Kravtsov 2005; Yang et al. 2005; Budzynski et al. 2012); still some claim that luminosity distribution is actually more concentrated (Koranyi et al. 1998; Carlberg et al. 2001).

Many of previous comparisons depend on probes of mass profiles based on real observational data, e.g. dynamical modelling methods (Carlberg et al. 1997; Rines et al. 2000; van der Marel et al. 2000; Carlberg et al. 2001; Rines et al. 2001; Tustin et al. 2001; Biviano & Girardi 2003; Łokas & Mamon 2003; Popesso et al. 2007), or X-ray observations (Cirimele et al. 1997; Lin et al. 2004; Budzynski et al. 2012). Mass estimation from these probes often requires some prior assumptions on the dynamical state of galaxy clusters/groups and thus may be biased. Weak lensing method is

★ E-mail: chunxiang_wang@sina.cn (CW); liran827@gmail.com (RL)

usually considered as an unbiased probe, which is independent of the dynamical states of galaxy clusters and baryonic physics in galaxy formation. In this work, we derive mass distribution of red-sequence Matched-filter Probabilistic Percolation (redMaPPer) clusters (Rozo & Rykoff 2014; Rykoff et al. 2014) using the high-quality weak lensing data from Canada–France–Hawaii Telescope (CFHT) Stripe 82 Survey (CS82; Li et al. 2014; Shan et al. 2014), and compare them directly with the satellite galaxies number density from SDSS Stripe 82 (Abazajian et al. 2009; Reis et al. 2012) photometric data.

The paper is laid out as follows. In Section 2, we describe the data used in our work. In Section 3, we describe lens model and how to get the satellite galaxy number density profile of our cluster sample. In Section 4, we show the results of this work. Finally, we summarize and discuss the implication of our results in Section 5. Throughout this paper, we adopt a flat ΛCDM cosmological model with the matter density parameter $\Omega_{\rm m} = 0.27$ and the Hubble parameter $H_0 = 70\,{\rm km\,s^{-1}Mpc^{-1}}$.

## 2 DATA

### 2.1 RedMaPPer cluster catalogue

The redMaPPer method (Rozo & Rykoff 2014; Rykoff et al. 2014) uses the *ugriz* magnitudes and their errors, to group spatial concentrations of red-sequence galaxies at similar redshift into cluster. In this paper, we use redMaPPer cluster catalogue extracted from SDSS DR8, restricting to the CS82 footprint, where high-quality weak lensing data are available. There are 634 clusters falling in this region. We further select our final cluster sample from these clusters using the following additional conditions: $0.1 \leq z \leq 0.33$, $20 < \lambda < 100$, and $P_{\rm cen} > 0.7$, where $z$ is the redshift of cluster, the $\lambda$ is an optical richness estimate indicating the number of red-sequence galaxies brighter than $0.2L_*$ at the redshift of the cluster within a scaled aperture which has been shown as a good mass proxy (Rykoff et al. 2012), and the $P_{\rm cen}$ is the probability of the most likely central galaxy. For each cluster, there are five candidate central galaxies and we always use the position of the most likely central galaxy as the proxy of the cluster centre. The redshift cut selects a nearly volume-limited cluster sample, the richness cut ensures a pure and statistically meaningful sample of clusters at all richness bins (Miyatake et al. 2016), and the probability cut reduces the miscentering problem. After applying these cuts, our final sample is composed of 167 clusters.

### 2.2 Lensing shear catalogue

The source galaxies used in this work are taken from CS82 survey which is an *i*-band imaging survey covering the SDSS Stripe 82 region with a median seeing 0.59 arcsec. The CS82 fields were observed in four dithered observations with a 410 s exposure. The limited magnitude is $i_{\rm AB} \sim 24.1$ (Battaglia et al. 2016).

The shapes of faint galaxies are measured with *lensfit* method (Miller et al. 2007, 2013). Each CS82 science image is supplemented by a mask, indicating regions within which accurate photometry/shape measurements of faint sources cannot be performed. According to Erben et al. (2013), most of science analyses are safe with $MASK \leq 1$. We use all galaxies with weight $\omega > 0$, FITCLASS=0, $MASK \leq 1$, and $z > 0$, in which $\omega$ represents an inverse variance weight assigned to each source galaxy by *lensfit*, FITCLASS is a star/galaxy classification provided by *lensfit*, and $z$ is the photometric redshift.

After masking out bright stars and other image artefacts, the effective survey area reduces from 173 deg$^2$ to 129.2 deg$^2$. As the CS82 is an *i*-band imaging survey, the photometric redshifts (photo-$z$) are obtained by using BPZ method (Benítez 2000; Coe et al. 2006) and computed by Bundy et al. (2015). Some tests on the systematics induced by photo-$z$ error are shown in Li et al. (2016). The total number of source galaxies in this work is 4381 917.

### 2.3 Satellite galaxy catalogue

To calculate the satellite galaxy number density of our cluster sample as described in Section 2.1, we download a photometric galaxy catalogue from SDSS Stripe 82 data base by requiring the magnitude of *r* band ($r_{\rm mag}$) in [17, 21] with the query provided by Reis et al. (2012). There are 1164 364 galaxies in the catalogue. By matching this photometric catalogue to the redMaPPer cluster catalogue with a matching tolerance of 1.0 arcsec, 'central galaxies' are identified in this photometric catalogue.

## 3 THEORY MODEL AND METHOD

### 3.1 Lensing model

We stack lens–source pairs in seven logarithmic radial $R$ bins from 0.03 to 1.5 Mpc. Lensing signal (excess surface density $\Delta\Sigma(R)$) is calculated by

$$\Delta\Sigma(R) = \overline{\Sigma(<R)} - \overline{\Sigma(R)} = \frac{\sum_{\rm ls}\omega_{\rm ls}\gamma_{\rm t}^{\rm ls}\Sigma_{\rm crit}}{\sum_{\rm ls}\omega_{\rm ls}}, \quad (1)$$

where

$$\omega_{\rm ls} = \omega_{\rm s}\Sigma_{\rm crit}^{-2}, \quad (2)$$

$$\Sigma_{\rm crit} = \frac{c^2}{4\pi G}\frac{D_{\rm s}}{D_{\rm l}D_{\rm ls}}, \quad (3)$$

$\overline{\Sigma(<R)}$ is the mean surface mass density within $R$, $\overline{\Sigma(R)}$ is the average surface density at the projected radius $R$, $\omega_{\rm s}$ is a weight factor introduced to account for intrinsic scatter in ellipticity and shape measurement error of each source galaxy, which is same with $\omega$ we mentioned in Section 2.1, $\Sigma_{\rm crit}$ is the critical surface density including space geometry information, $D_{\rm s}$ and $D_{\rm l}$ are the angular diameter distances of source and lens, respectively, $D_{\rm ls}$ is the angular diameter distance between source and lens, and $\gamma_{\rm t}$ is the tangential shear.

We apply a correction to lensing signal computed from the multiplicative shear calibration factor $m$ as in Velander et al. (2014):

$$1 + K(z_{\rm l}) = \frac{\sum_{\rm ls}\omega_{\rm ls}(1+m)}{\sum_{\rm ls}\omega_{\rm ls}}. \quad (4)$$

Weak lensing signal can finally be obtained by

$$\Delta\Sigma^{\rm cal}(R) = \frac{\Delta\Sigma(R)}{1 + K(z_{\rm l})}. \quad (5)$$

Owing to large photo-$z$ uncertainties of the source galaxies, we remove the lens–source pairs with $z_{\rm s} - z_{\rm l} < \sigma_z$, where $\sigma_z$ represents a $1\sigma$ error of photo-$z$.

The weak lensing signal is modelled as

$$\Delta\Sigma(R) = \frac{M_{\rm star}}{\pi R^2} + P_{\rm cc}\Delta\Sigma_{\rm NFW}(R) + (1 - P_{\rm cc})\Delta\Sigma_{\rm NFW}^{\rm off}(R), \quad (6)$$

where the first term represents the contribution of the stellar mass of the central galaxy, the second and third terms represent the perfectly

centred and miscentered component of dark matter haloes (and also the diffused baryonic matter like hot gas), respectively.

We model the central galaxy as a point mass following Leauthaud et al. (2012) and fix $M_{\rm star}$ to the average mass of central galaxies. Stellar masses are estimated for member galaxies in the redMaPPer catalogue using the Bayesian spectral energy distribution modelling code ISEDFIT (Moustakas et al. 2013). $P_{\rm cc}$ and $(1-P_{\rm cc})$ are weights for the centred and miscentering part of the dark matter halo surface mass density, respectively.

Dark matter density profile is described by the Navarro, Frenk & White (1997, hereafter NFW) profile

$$\rho(r) \propto \frac{1}{(r/r_{\rm s})(1+r/r_{\rm s})^2}, \tag{7}$$

where $r_{\rm s}$ is the scale radius which is commonly quantified in terms of the concentration parameter $C_{200} = R_{200}/r_{\rm s}$, where $R_{200}$ is the virial radius enclosing the virial mass $M_{200} = (800/3)\pi R_{200}^3 \rho_{\rm c}$, where $\rho_{\rm c}$ is the critical density of the universe at the redshift of the halo.

By integrating the three-dimensional (3D) density profile along the line of sight, we can get the projected surface density $\Sigma_{\rm NFW}(R)$ which is a function of the projection radius $R$

$$\Sigma_{\rm NFW}(R) = \int_0^\infty \rho\left(\sqrt{R^2+z^2}\right) {\rm d}z. \tag{8}$$

Integrating $\Sigma_{\rm NFW}(R)$ from 0 to $R$, we can get the mean surface density within $R$, $\overline{\Sigma_{\rm NFW}(<R)}$

$$\overline{\Sigma_{\rm NFW}(<R)} = \frac{2}{R^2}\int_0^R R'\Sigma_{\rm NFW}(R'){\rm d}R'; \tag{9}$$

here, $\rho$ is the NFW density profile.

There are possibilities that BCG may be misidentified in the cluster catalogue, so we are also including a '*miscentering*' term. If the central galaxy is offset from the halo centre by a distance $R_{\rm mc}$, the mass surface density will be changed as follows:

$$\Sigma_{\rm NFW}(R|R_{\rm mc}) = \int_0^{2\pi} {\rm d}\theta \Sigma_{\rm NFW}\left(\sqrt{R^2+R_{\rm mc}^2+2RR_{\rm mc}\cos(\theta)}\right). \tag{10}$$

The distribution of miscentering can be described by a 2D Gaussian distribution

$$P(R_{\rm mc}) = \frac{R_{\rm mc}}{\sigma_{\rm off}^2}\exp\left(-\frac{1}{2}\left(\frac{R_{\rm mc}}{\sigma_{\rm off}}\right)^2\right). \tag{11}$$

In the fitting model, there are four free parameters, $M_{200}$, $C_{200}$, $\sigma_{\rm off}$, and $P_{\rm cc}$. Due to the strong degeneracy between $\sigma_{\rm off}$ and $P_{\rm cc}$, our data are not good enough to fit $\sigma_{\rm off}$ and $P_{\rm cc}$ well synchronously (see the results in Appendix). We assume that the position of one of the five central galaxy candidates is true centre of the galaxy cluster, so we fix $\sigma_{\rm off}$ and $P_{\rm cc}$ in following way.

First, we fix $P_{\rm cc} = 0.95$ to the average of $P_{\rm cen}$ of 167 clusters sample we finally select. Secondly, we fit the distribution of the candidates of the central galaxy to obtain $\sigma_{\rm off}$. There are five candidates of the central galaxy. We calculate the distribution of the projected distance between the most likely central galaxy and the four remaining central candidate galaxies, and fit this distribution with equation (11). As shown in Fig. 1, the red histogram shows the distribution of miscentering and the blue solid line represents the best-fitting curve. The best-fitting effective scale length is $\sigma_{\rm off} = (0.095 \pm 0.002)$ Mpc.

As a comparison, we also show the four free parameters model fitting results in Appendix.

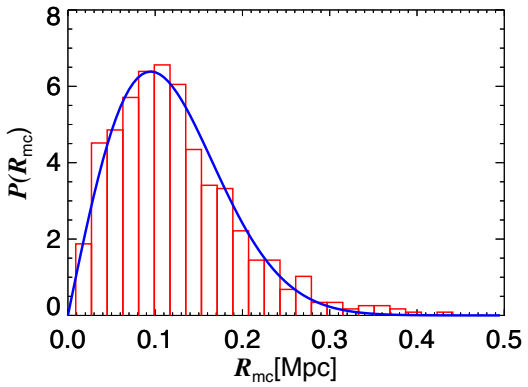


**Figure 1.** The distribution of miscentering. We take the projected distance between the most likely central galaxy and the four remaining central candidate galaxies as $R_{\rm mc}$. The red histogram shows the distribution of $R_{\rm mc}$. The blue line is the best-fitting curve of the distribution of $R_{\rm mc}$.

Substituting equation (11) into following equation (12), we can obtain the resulting mean surface mass profile for the miscentered clusters.

$$\Sigma_{\rm NFW}^{\rm off}(R) = \int {\rm d}R_{\rm mc} P(R_{\rm mc})\Sigma_{\rm NFW}(R|R_{\rm mc}). \tag{12}$$

There are two free parameters, $M_{200}$ and $C_{200}$, in our lensing fitting model.

### 3.2 Satellite number density

For each central galaxy, we count the number of galaxies in $r$-band magnitude range $17 < r_{\rm mag} < 21$ and not brighter than the central galaxy in different projected radial bins. These galaxies contain satellites and galaxies in the background or foreground.

To compare directly with the weak lensing measurement, we calculate $\Delta\Sigma_{\rm g}(R)$ instead of $\Sigma_{\rm g}(R)$

$$\Delta\Sigma_{\rm g}(R) = \overline{\Sigma_{\rm g}(<R)} - \overline{\Sigma_{\rm g}(R)}, \tag{13}$$

where $\overline{\Sigma_{\rm g}(<R)}$ represents galaxy surface number density within $R$, and $\overline{\Sigma_{\rm g}(R)}$ is the average galaxy surface number density at the projected radius $R$ and each of them contains the background galaxy density. So naturally the background is cancelled when we stack a lot of clusters. We calculate $\Delta\Sigma_{\rm g}(R)$ for each individual cluster and average over the whole sample.

We assume the number density of galaxies also follows an NFW form as

$$N(r) = \frac{N_0}{(r/r_{\rm s,gal})(1+r/r_{\rm s,gal})^2}. \tag{14}$$

The satellite galaxy surface number density fitting model includes the two components

$$\Delta\Sigma_{\rm g}(R) = P_{\rm cc}\Delta\Sigma_{\rm g}^{\rm cen}(R) + (1-P_{\rm cc})\Delta\Sigma_{\rm g}^{\rm off}(R). \tag{15}$$

The two terms on the right-hand side of the equation represent centred and miscentering NFW profile, respectively. $N_0$ and $r_{\rm s}$ are free parameters in our fitting. Owing to the same centre we used both in weak lensing signal calculation and satellite galaxy count, the satellite number density profile shares the same $\sigma_{\rm off}$ and $P_{\rm cc}$ with density of mass. We fix $\sigma_{\rm off} = 0.095$ Mpc and $P_{\rm cc} = 0.95$.

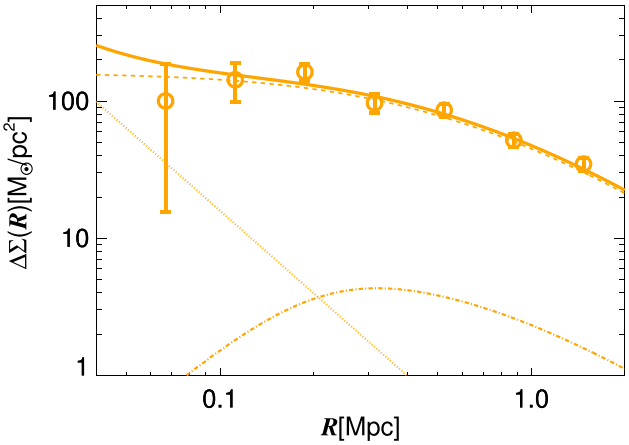


**Figure 2.** Best-fitting model for weak lensing of 167 clusters. The orange circles represent the excess surface mass density $\Delta\Sigma(R)$ of cluster sample. Errors bars reflect the 68 per cent confidence intervals obtained using bootstrapping. The solid line shows the best-fitting model. The dashed line is the centred dark matter halo term. The dot–dashed line is the miscentering dark matter halo term and the dotted line corresponds to the stellar mass contribution from the central galaxy. The corresponding best-fitting parameters are listed in Table 1.

**Table 1.** Best-fitting parameters of the mass profile from fitting the weak lensing data.

| $M_{200}/10^{14}\,M_\odot$ | $C_{200}$ | $M_{\rm star}/10^{11}\,M_\odot$ | $r_{\rm s}$/Mpc | $\chi^2$/dof |
|---|---|---|---|---|
| $2.06^{+0.61}_{-0.41}$ | $2.80^{+0.81}_{-0.67}$ | 4.99 | $0.37^{+0.15}_{-0.10}$ | 4.15/5 |

## 4 RESULTS

With the Markov Chain Monte Carlo technique, we can fit the weak lensing signal and the satellite galaxy number density to get the posterior distribution of the free parameters.

In Fig. 2, we show the stacked lensing signal of our cluster sample. The orange circles with errors bars represent weak lensing signal and errors bars reflect the 68 per cent confidence intervals obtained by bootstrapping. The bold solid line shows the best-fitting model, the dashed line is the centred dark matter halo term, the dot–dashed line is the miscentering dark matter halo term, and the dotted line corresponds to the stellar mass contribution from central galaxy. The best-fitting parameters are listed in Table 1. We obtain a halo mass $M_{200} = 2.06^{+0.61}_{-0.41} \times 10^{14}\,M_\odot$ that is consistent with the halo mass fitting result in Miyatake et al. (2016), as well as the halo mass estimated by mass-richness relation in Melchior et al. (2017) and Shan et al. (2017) within a $1\sigma$ error. The fitted scale radius is $r_{\rm s} = 0.37^{+0.15}_{-0.10}$ Mpc. The concentration parameter obtained here is $C_{200} = 2.80^{+0.81}_{-0.67}$. To compare our measurements with the 3D $N$-body simulation results directly, we correct the $C_{200}$ with the 3D correction in Giocoli et al. (2012)

$$C_{\rm 2D}(M) = C_{\rm 3D}(M) \times 1.630 M^{-0.018}, \quad (16)$$

and rescale the concentration parameter to $z = 0$ with the redshift dependence in Klypin et al. (2016). We get the corrected concentration parameter $C_{200,\rm 3D} = 3.62^{+1.07}_{-0.88}$, which is consistent with the prediction from cosmological simulations provided by Klypin et al. (2016) within a $1\sigma$ error.

In Fig. 3, we show the excess surface number density of satellite galaxy of our cluster sample. The deep pink circles with errors bars are the satellite galaxy excess number surface density. The solid line represents the best-fitting model. The dashed line is the centred term and the dot–dashed line is the miscentering term. Fitting results of excess surface number density are listed in Table 2.

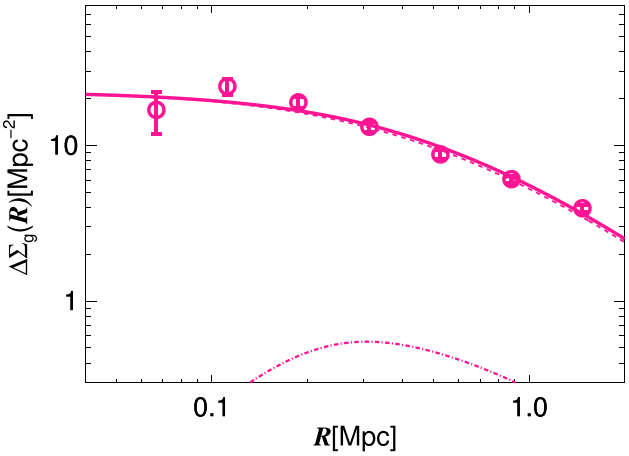


**Figure 3.** Best-fitting model for galaxy number density of 167 clusters. The deep pink circles with errors bars represent the excess surface number density $\Delta\Sigma_{\rm g}(R)$ of cluster sample. The solid line represents the best-fitting model. The dashed line is the centred term and the dot–dashed line is the miscentering term. The corresponding best-fitting parameters are listed in Table 2.

**Table 2.** Best-fitting parameters of the galaxy density profile.

| $N_0/{\rm Mpc}^{-3}$ | $r_{\rm s,gal}$/Mpc | $C_{\rm g}$ | $\chi^2$/dof |
|---|---|---|---|
| $68.17^{+13.60}_{-11.26}$ | $0.34^{+0.04}_{-0.03}$ | $3.03 \pm 0.30$ | 12.27/5 |

We compare the satellite galaxy excess surface number density $\Delta\Sigma_{\rm g}(R)$ with the mass excess surface density $\Delta\Sigma(R)$ directly in Fig. 4. To compare their profiles intuitively, we divide 8.5 into $\Delta\Sigma(R)$ to obtain a similar amplitude with $\Delta\Sigma_{\rm g}(R)$. As shown in Fig. 4, they have a similar distribution. We find that the fitted scale radius with satellite galaxy excess surface number density $r_{\rm s,gal} = 0.34^{+0.04}_{-0.03}$ Mpc ($C_{\rm g} = 3.03 \pm 0.30$) is consistent with the scale radius $r_{\rm s} = 0.37^{+0.15}_{-0.10}$ Mpc ($C_{200} = 2.80^{+0.81}_{-0.67}$) fitted with weak lensing signal within a $1\sigma$ error showing that the satellite galaxy number density profile traces mass distribution closely in the galaxy clusters.

In some previous studies, the generalized NFW or the Einasto parametric profile model is also used to fit the mass density or satellite galaxies number density profile (Łokas & Mamon 2003; More et al. 2016). In this paper, only the NFW profile model is adopted. Thus, we also compare these two profiles in a non-parametric way without any model dependence. In Fig. 5, we show the distribution of number-to-mass ratio with the projected radius $R$. Errors bars represent the $1\sigma$ uncertainties. The shaded region is standard errors of the number-to-mass ratio. The number-to-mass ratio is nearly a constant within a $1\sigma$ error. Note that the number-to-mass ratio is still nearly a constant when projected distances are scaled by virial radii from the mass-richness scaling relation in Simet et al. (2017).

## 5 SUMMARY

In this short paper, we perform a comparison between the satellite number density profile and mass profile of redMaPPer clusters. For the mass profile, we select a sample of 167 redMaPPer clusters in the CS82 area with $20 < \lambda < 100$, $0.1 \leq z \leq 0.33$, and $P_{\rm cen} > 0.7$ and calculate the stacked weak lensing signal around them to obtain

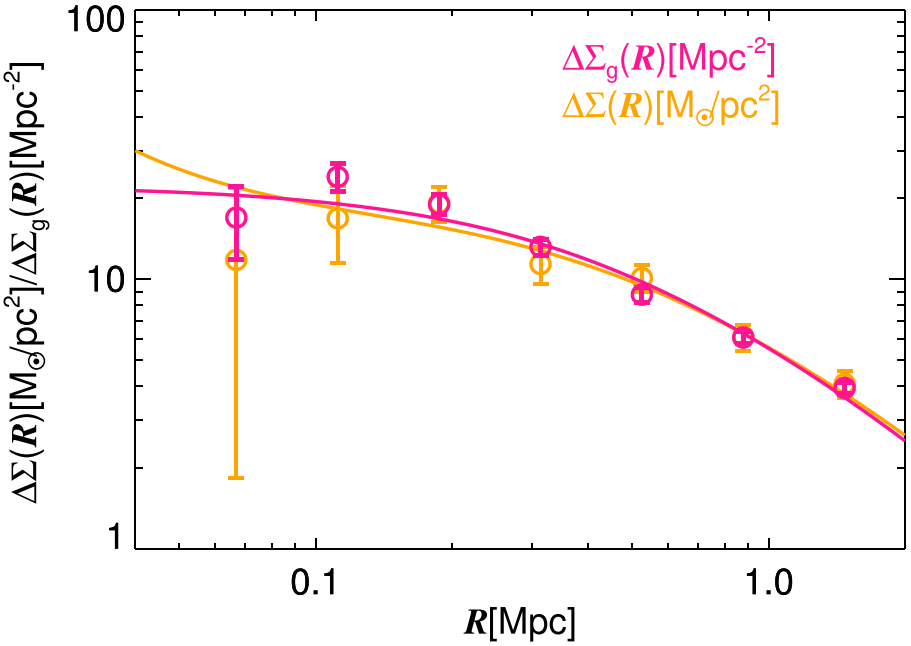


**Figure 4.** A comparison between mass distribution and galaxy number density profile. The deep pink circles with errors bars correspond to the satellite galaxy excess surface number density $\Delta\Sigma_g(R)$ and the deep pink solid line represents the best-fitting model. Orange circles represent excess mass surface density $\Delta\Sigma(R)$ and the solid orange lines represent the best-fitting model. Errors bars reflect $1\sigma$ uncertainties. Here, we divided 8.5 into $\Delta\Sigma(R)$ to get a similar amplitude with $\Delta\Sigma_g(R)$. Satellite galaxies are selected by $17 < r_{mag} < 21$.

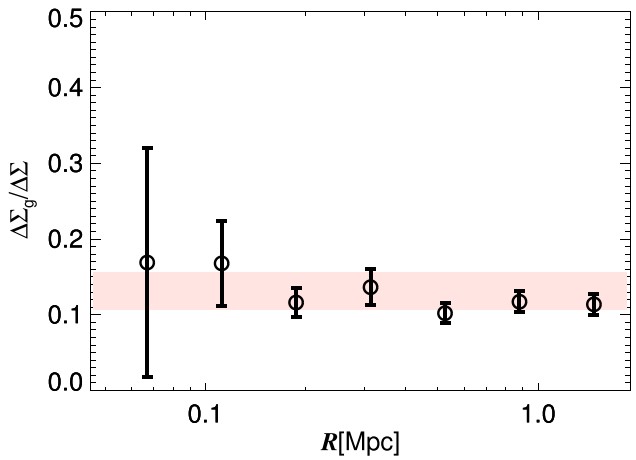


**Figure 5.** The distribution of number-to-mass ratio. Errors bars reflect the $1\sigma$ uncertainties. The shaded region is standard errors of the number-to-mass ratio.

the mass distribution from 0.03 to 1.5 Mpc. We extract the satellite galaxies in the same cluster sample using SDSS Stripe 82 photometric data in the *r*-band magnitude range $17 < r_{mag} < 21$. Comparing the excess surface mass density with the satellite galaxy number density, we find that they agree with each other well and both can be fitted with the NFW profile. The best-fitting scale radius $r_s$ and concentration parameter $C$ of these two profiles are consistent with each other within a $1\sigma$ error, thus we can conclude that the satellite galaxy number density is an unbiased tracer of mass distribution in galaxy clusters. Our conclusion is consistent with some similar studies using observational data based on dynamical methods (e.g. Carlberg et al. 1997; van der Marel et al. 2000; Biviano & Girardi 2003) or based on the other methods (e.g. Cirimele et al. 1997; Parker et al. 2005; Sereno et al. 2010).

## ACKNOWLEDGEMENTS

We are indebted to the referee for the thoughtful comments and insightful suggestions that improved this paper greatly. We acknowledge support from the National Key Program for Science and Technology Research and Development (2017YFB0203300). RL acknowledges NSFC grant (nos. 11773032, 11333001), support from the Youth Innovation Promotion Association of CAS, Youth Science funding of NAOC, and Nebula Talent Program of NAOC. LG acknowledges support from the NSFC grant (nos. 11133003, 11425312), and a Newton Advanced Fellowship, as well as the hospitality of the Institute for Computational Cosmology at Durham University. HYS and JPK acknowledge support from the ERC advanced grant LIDA. CXW and GC acknowledge NSFC grant no. 10903006, and support from the Middle-aged and Young Key Innovative Talents Program for Universities in Tianjin. M. Makler is partially supported by CNPq and FAPERJ Fora Temer. T. Erben is supported by the Deutsche Forschungsgemeinschaft in the framework of the TR33 'The DarkUniverse'.

Based on observations obtained with MegaPrime/MegaCam, a joint project of CFHT and CEA/DAPNIA, at the CFHT, which is operated by the National Research Council (NRC) of Canada, the Institut National des Science de l'Univers of the Centre National de la Recherche Scientifique (CNRS) of France, and the University of Hawaii. The Brazilian partnership on CFHT is managed by the Laboratrio Nacional de Astronomia (LNA). This work made use of the CHE cluster, managed and funded by ICRA/CBPF/MCTI, with financial support from FINEP and FAPERJ. We thank the support of the Laboratrio Interinstitucional de e-Astronomia (LIneA).

We thank the CFHTLenS team for their pipeline development and verification upon which much of this surveys pipeline was built.

## REFERENCES


Abazajian K. N. et al., 2009, ApJS, 182, 543
Bahcall N. A., Kulier A., 2014, MNRAS, 439, 2505
Battaglia N. et al., 2016, J. Cosmology Astropart. Phys., 8, 013
Benítez N., 2000, ApJ, 536, 571
Biviano A., Girardi M., 2003, ApJ, 585, 205
Budzynski J. M., Koposov S. E., McCarthy I. G., McGee S. L., Belokurov V., 2012, MNRAS, 423, 104
Bundy K. et al., 2015, ApJS, 221, 15
Carlberg R. G., Yee H. K. C., Ellingson E., 1997, ApJ, 478, 462
Carlberg R. G., Yee H. K. C., Morris S. L., Lin H., Hall P. B., Patton D. R., Sawicki M., Shepherd C. W., 2001, ApJ, 552, 427
Cirimele G., Nesci R., Trèvese D., 1997, ApJ, 475, 11
Coe D., Benítez N., Sánchez S. F., Jee M., Bouwens R., Ford H., 2006, AJ, 132, 926
Diemand J., Moore B., Stadel J., 2004, MNRAS, 352, 535
Erben T. et al., 2013, MNRAS, 433, 2545
Fischer P., Tyson J. A., 1997, AJ, 114, 14
Gao L., De Lucia G., White S. D. M., Jenkins A., 2004, MNRAS, 352, L1
Giocoli C., Meneghetti M., Ettori S., Moscardini L., 2012, MNRAS, 426, 1558
Hansen S. M., McKay T. A., Wechsler R. H., Annis J., Sheldon E. S., Kimball A., 2005, ApJ, 633, 122
Klypin A., Yepes G., Gottlöber S., Prada F., Heß S., 2016, MNRAS, 457, 4340
Kneib J.-P. et al., 2003, ApJ, 598, 804
Koranyi D. M., Geller M. J., Mohr J. J., Wegner G., 1998, AJ, 116, 2108
Leauthaud A. et al., 2012, ApJ, 744, 159
Li R. et al., 2014, MNRAS, 438, 2864
Li R. et al., 2016, MNRAS, 458, 2573
Lin Y.-T., Mohr J. J., Stanford S. A., 2004, ApJ, 610, 745
Łokas E. L., Mamon G. A., 2003, MNRAS, 343, 401
Melchior P. et al., 2017, MNRAS, 469, 4899
Miller L., Kitching T. D., Heymans C., Heavens A. F., van Waerbeke L., 2007, MNRAS, 382, 315
Miller L. et al., 2013, MNRAS, 429, 2858
Miyatake H., More S., Takada M., Spergel D. N., Mandelbaum R., Rykoff E. S., Rozo E., 2016, Phys. Rev. Lett., 116, 041301
More S. et al., 2016, ApJ, 825, 39
Moustakas J. et al., 2013, ApJ, 767, 50
Nagai D., Kravtsov A. V., 2005, ApJ, 618, 557
Navarro J. F., Frenk C. S., White S. D. M., 1997, ApJ, 490, 493 (NFW)
Parker L. C., Hudson M. J., Carlberg R. G., Hoekstra H., 2005, ApJ, 634, 806
Popesso P., Biviano A., Böhringer H., Romaniello M., 2007, A&A, 464, 451
Reis R. R. R. et al., 2012, ApJ, 747, 59
Rines K., Geller M. J., Diaferio A., Mohr J. J., Wegner G. A., 2000, AJ, 120, 2338
Rines K., Geller M. J., Kurtz M. J., Diaferio A., Jarrett T. H., Huchra J. P., 2001, ApJ, 561, L41
Rozo E., Rykoff E. S., 2014, ApJ, 783, 80
Rykoff E. S. et al., 2012, ApJ, 746, 178
Rykoff E. S. et al., 2014, ApJ, 785, 104
Sereno M., Lubini M., Jetzer P., 2010, A&A, 518, A55
Shan H. Y. et al., 2014, MNRAS, 442, 2534
Shan H. et al., 2017, ApJ, 840, 104
Sheldon E. S. et al., 2009, ApJ, 703, 2232
Simet M., McClintock T., Mandelbaum R., Rozo E., Rykoff E., Sheldon E., Wechsler R. H., 2017, MNRAS, 466, 3103
Springel V., White S. D. M., Tormen G., Kauffmann G., 2001, MNRAS, 328, 726
Squires G., Kaiser N., Fahlman G., Babul A., Woods D., 1996, ApJ, 469, 73
Tustin A. W., Geller M. J., Kenyon S. J., Diaferio A., 2001, AJ, 122, 1289
Tyson J. A., Fischer P., 1995, ApJ, 446, L55
van der Marel R. P., Magorrian J., Carlberg R. G., Yee H. K. C., Ellingson E., 2000, AJ, 119, 2038
Velander M. et al., 2014, MNRAS, 437, 2111
Vogelsberger M. et al., 2014, Nature, 509, 177
Wang W., Sales L. V., Henriques B. M. B., White S. D. M., 2014, MNRAS, 442, 1363
Wojtak R., Łokas E. L., 2010, MNRAS, 408, 2442
Yang X., Mo H. J., van den Bosch F. C., Weinmann S. M., Li C., Jing Y. P., 2005, MNRAS, 362, 711


## APPENDIX: FOUR FREE PARAMETERS MODEL

In the lensing model, we can also treat $\sigma_{\rm off}$ and $P_{\rm cc}$ as free parameters. Thus, we have four free parameters in the fitting model, $M_{200}$, $C_{200}$, $\sigma_{\rm off}$, and $P_{\rm cc}$. We show the 68 and 95 per cent confidence intervals for the four free parameters in Fig. A1. The last panel in each row shows the marginalized posterior distribution and the red solid lines represent the best-fitting parameters. The red dashed lines are the $1\sigma$ error of $\sigma_{\rm off}$ and $P_{\rm cc}$. The blue dashed lines represent the value of $\sigma_{\rm off}$ and $P_{\rm cc}$ in our two-parameter model.

For weak lensing data fitting, we obtain a halo mass $M_{200} = 2.15^{+0.38}_{-0.32} \times 10^{14}\,{\rm M}_{\odot}$ and concentration parameter $C_{200} = 2.63^{+1.80}_{-0.61}$ which are consistent with our two-parameter model results in Section 3.1 within a $1\sigma$ error. The best-fitting results are listed in Table A1.

As the satellite number density shares the same $\sigma_{\rm off}$ and $P_{\rm cc}$ with density of mass, we thus fix the two parameters to the best-fitting value from weak lensing data for the satellite number density fitting. We show the best-fitting model of satellite number density in Table A2. Again, the best-fitting scale radius from the galaxy density profile agrees with that from the lensing data (see Fig. A2).

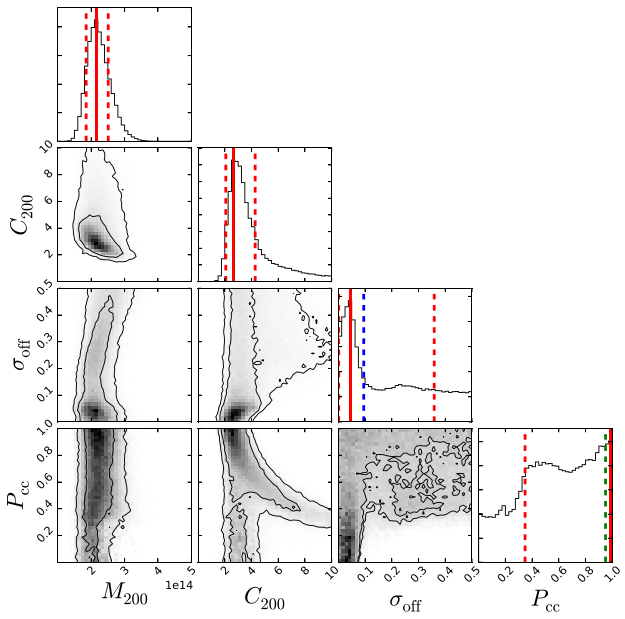


**Figure A1.** The 68 and 95 per cent confidence intervals for the four free parameters, $M_{200}$, $C_{200}$, $\sigma_{\rm off}$, and $P_{\rm cc}$. $M_{200}$ and $\sigma_{\rm off}$ are in units of $\rm M_{\odot}$ and Mpc, respectively. The last panel in each row shows the marginalized posterior distribution and the red solid lines represent the best-fitting parameters. The red dashed lines are the $1\sigma$ error of $\sigma_{\rm off}$ and $P_{\rm cc}$. The blue dashed line is $\sigma_{\rm off} = (0.095 \pm 0.002)$ Mpc and the green dashed line is $P_{\rm cc} = 0.95$ which are the values we used in our two-parameter model.

**Table A1.** Best-fitting parameters of the mass profile from fitting the weak lensing data.

| $M_{200}/10^{14}\,M_\odot$ | $C_{200}$ | $M_{\rm star}/10^{11}M_\odot$ | $\sigma_{\rm off}$/Mpc | $P_{\rm cc}$ | $r_{\rm s}$/Mpc | $\chi^2$/dof |
|---|---|---|---|---|---|---|
| $2.15^{+0.38}_{-0.32}$ | $2.63^{+1.80}_{-0.61}$ | 4.99 | $0.04^{+0.32}_{-0.04}$ | $0.99^{+0.01}_{-0.64}$ | $0.32^{+0.10}_{-0.14}$ | 3.967/3 |

**Table A2.** Best-fitting parameters of the galaxy density profile.

| $N_0$/Mpc$^{-3}$ | $r_{\rm s,gal}$/Mpc | $C_{\rm g}$ | $\chi^2$/dof |
|---|---|---|---|
| $64.353^{+12.41}_{-10.47}$ | $0.35^{+0.04}_{-0.03}$ | $2.98 \pm 0.17$ | 11.342/5 |

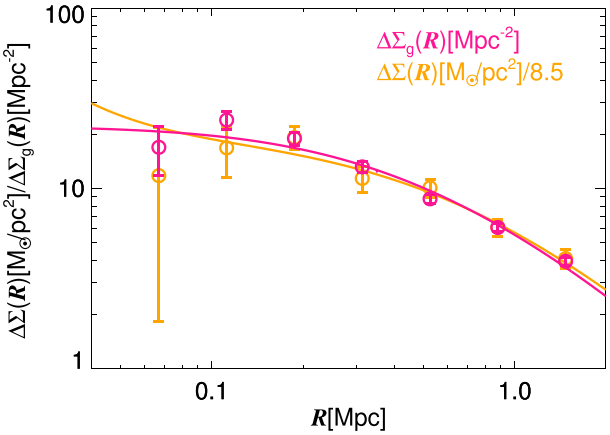


**Figure A2.** Similar figure to Fig. 4, but with four free parameters.

This paper has been typeset from a TEX/LATEX file prepared by the author.